

Experimental study of the Γ - X electron transfer in type-II (Al,Ga)As/AlAs superlattices and multiple-quantum-well structures

J. Feldmann

Fachbereich Physik, Philipps-Universität Marburg, Renthof 5, D-3550 Marburg, Federal Republic of Germany

J. Nunnenkamp

Max-Planck-Institut für Festkörperforschung, Heisenbergstrasse 1, Postfach 80 06 65, D-7000 Stuttgart 80, Federal Republic of Germany

G. Peter and E. Göbel

Fachbereich Physik, Philipps-Universität Marburg, Renthof 5, D-3550 Marburg, Federal Republic of Germany

J. Kuhl and K. Ploog

Max-Planck-Institut für Festkörperforschung, Heisenbergstrasse 1, Postfach 80 06 65, D-7000 Stuttgart 80, Federal Republic of Germany

P. Dawson and C. T. Foxon

Philipp Research Laboratories, Redhill, Surrey RH1 5HA, United Kingdom

(Received 2 March 1990)

A detailed experimental study of the real-space Γ - X transfer in type-II GaAs/AlAs short-period superlattices and in type-II $\text{Al}_x\text{Ga}_{1-x}\text{As}/\text{AlAs}$ multiple-quantum-well structures is presented. Transfer times on a subpicosecond and picosecond time scale are observed. The time constants critically depend on the thickness of the (Al,Ga)As layers, but not on the AlAs-layer thickness in the samples studied. The Γ - X transfer rate is determined by the spatial overlap of the Γ and X wave functions confined in the different layers. Intensity- and temperature-dependent measurements provide insight into the scattering mechanism. We conclude that electron-LO-phonon scattering is the dominant scattering process for samples with thick (Al,Ga)As layers ($> 100 \text{ \AA}$). In contrast, interface scattering due to the interface mixing potential (Γ - X_z mixing) and/or due to potential fluctuations caused by interface roughness (Γ - $X_{x,y}$ mixing) probably dominates for samples with thin (Al,Ga)As layers ($< 35 \text{ \AA}$).

I. INTRODUCTION

The electrical and optical properties of semiconductor materials are strongly influenced by carrier-scattering processes. The relative importance of different scattering mechanisms, e.g., carrier-carrier, carrier-phonon, carrier-defect, or carrier-impurity interaction, as well as their respective scattering rates, depends on band structure, excess energy of the excited carriers, carrier density, and the interaction potential of the relevant mechanism.

The recent progress in high-speed electronic semiconductor devices^{1,2} and very large-scale integration has stimulated intensive research on intervalley-scattering phenomena.³⁻⁸ Under the influence of high electric fields applied in ultrafast electronic devices, electrons in the lowest conduction-band minimum (e.g., at the Γ point for GaAs) can be effectively scattered to higher valleys, e.g., to the X and L points of the Brillouin zone for GaAs. These scattering processes are of fundamental importance for high-speed electronic devices, since the transfer of carriers from Γ to, e.g., the X valleys results in a drastic reduction of the carrier mobility, owing to the large effective mass of carriers in the satellite valleys.

Several groups have investigated Γ - X intervalley scattering of electrons in bulk semiconductors GaAs and $\text{Al}_x\text{Ga}_{1-x}\text{As}$ (Refs. 4 and 6-8) and measured scattering times as short as 30-80 fs.^{4,6,7} It is evident that the Γ - X scattering rate will vary as a function of the excess energy of the electron in the Γ valley with respect to the energy of the X minimum, and thus critically depends upon the band structure. The recent progress in growing quantum-well and superlattice (SL) structures provides great potential for tailoring these scattering rates.

Variation of the GaAs well width in a $(\text{GaAs})_m/(\text{AlAs})_n$ SL (m, n give the number of monolayers with thickness $a_0 = 2.83 \text{ \AA}$) results in an increased confinement energy of the Γ conduction-band states in the GaAs layer with decreasing well width, if coupling between adjacent wells is not significant. This allows us to tune the lowest Γ conduction-band state in the GaAs to lie above the X minima of the AlAs layers and generate a type-II SL configuration for $m \leq 12$. In these type-II SL's, the highest valence-band state is contained in the GaAs layers, whereas the lowest conduction-band state occurs in the AlAs layers. In ternary- on binary-compound $(\text{Al}_x\text{Ga}_{1-x}\text{As})_m/(\text{AlAs})_n$ SL's, type-II behav-

ior can be maintained for any thickness, provided that the composition x is chosen properly. The optical properties of type-II (Al,Ga)As/AlAs SL's have been extensively studied by several groups.^{9–17}

A unique process occurs in these type-II SL's; intervalley electron scattering additionally involves a real-space transfer of the carriers from the $\text{Al}_x\text{Ga}_{1-x}\text{As}$ layer across the interface to the AlAs layer. It was shown recently that the Γ - X scattering rate in all binary $(\text{GaAs})_m/(\text{AlAs})_n$ type-II short-period superlattices (SPS's) can be extremely high and comparable to the Γ - X scattering rate in a GaAs bulk crystal,^{18,19} in spite of the spatial charge transfer. $(\text{Al}_x\text{Ga}_{1-x}\text{As})_m/(\text{AlAs})_n$ multiple-quantum-well (MQW) structures which show type-II behavior for much larger values of m permit extension of such studies to a much broader range of well thickness.^{20,21}

In this paper we present a systematic study of the Γ - X intervalley scattering in $(\text{Al}_x\text{Ga}_{1-x}\text{As})_m/(\text{AlAs})_n$ type-II SL's and MQW's grown by molecular-beam epitaxy (MBE) with various values for x , m , and n using picosecond and femtosecond excite and probe spectroscopy. We demonstrate that the scattering rate can systematically be varied within a broad range (100 fs to 22 ps) by changing the geometrical dimensions of the sample structure and the composition of the well material. Our results reveal that the scattering rate depends on the spatial overlap of the electron wave functions of the Γ minimum of the $\text{Al}_x\text{Ga}_{1-x}\text{As}$ layer and of the X minima of the AlAs layer.

Comprehensive studies of the scattering times with varying excitation intensity and sample temperature provide information about the nature of the scattering mechanism. Our experimental data indicate that interface scattering due to Γ - X_z and/or Γ - $X_{x,y}$ mixing is dominant for thin GaAs layers ($m \leq 12$). This mechanism is expected to decrease with increasing well width, in accordance with the decrease of the probability amplitude of the electron wave function at the interface. Consistently, the temperature-dependent measurements show that electron-phonon scattering becomes the dominant scattering mechanism for thick $\text{Al}_x\text{Ga}_{1-x}\text{As}$ layers ($m > 35$).

The paper is organized as follows. In Sec. II we will briefly summarize the electronic features of type-II SPS's and discuss their optical properties. Nonresonant and resonant transient pump and probe experiments have been used to study the fast scattering of electrons from Γ -related to X -related states for nine GaAs/AlAs and three $\text{Al}_x\text{Ga}_{1-x}\text{As}/\text{AlAs}$ samples; in Sec. III the experimental results at low temperature are presented. In Sec. III A we demonstrate that the experimentally determined Γ - X transfer times for the type-II GaAs/AlAs SPS's drastically increase with increasing GaAs layer thickness, but are almost independent of the AlAs layer thicknesses. Results from the type-II $\text{Al}_x\text{Ga}_{1-x}\text{As}/\text{AlAs}$ multiple quantum wells are presented in Sec. III B. In Sec. IV we show that the overlap of the Γ and X envelope wave functions determines the Γ - X transfer rate. Finally, in Sec. V the underlying scattering mechanisms responsible for the Γ - X real-space transfer are discussed. We conclude that

electron-LO-phonon interaction is the dominant scattering mechanism for samples with thick layers ($> 100 \text{ \AA}$), whereas for those with thin layers ($< 35 \text{ \AA}$) interface scattering becomes dominant.

II. ELECTRONIC AND OPTICAL PROPERTIES

The band alignment of a so-called type-I GaAs/AlAs superlattice is characterized by the fact that the lowest conduction-band states and the highest valence-band states are in the same material (GaAs). Consequently, electrons in the conduction band and holes in the valence band both find their lowest-energy states in the GaAs layer. In contrast, in type-II superlattices the lowest-energy states for photoexcited electrons and holes are located in different layers. For type-II (Al,Ga)As/AlAs superlattices, the lowest-lying electronic states of the conduction band are confined in the AlAs layers, whereas the highest-lying states of the valence band are confined in the (Al,Ga)As layers, as shown in Fig. 1. This staggered band alignment is achieved if the confinement energy of the lowest Γ level in the (Al,Ga)As becomes sufficiently high, which in $(\text{GaAs})_m/(\text{AlAs})_n$ SPS's is fulfilled for m smaller than 12.¹⁶ Type-II behavior can be maintained in the ternary- on binary-compound $(\text{Al}_x\text{Ga}_{1-x}\text{As})_m/(\text{AlAs})_n$ superlattice for any thickness, provided the composition x is chosen properly.¹⁰

The Γ - and X -band alignments along the growth axis [001] (the z axis) of the superlattice are treated independently in the simplest theoretical approach. In the envelope-function approximation, the Γ and X energy eigenvalues and wave functions are calculated on the basis of the Kronig-Penney model using the respective effective masses in z direction.²² Due to the anisotropy of the X minimum in AlAs ($m_l = 1.1m_0, m_t = 0.2m_0$), two

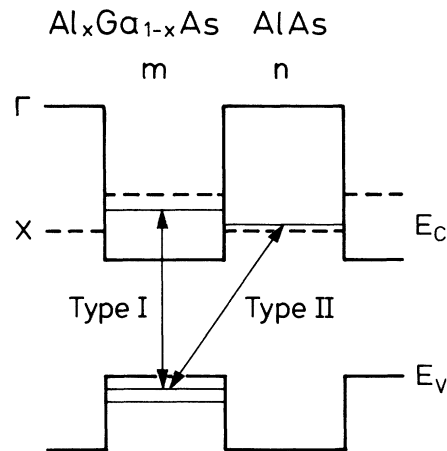


FIG. 1. Band scheme of a type-II (Al,Ga)As/AlAs superlattice in growth direction z . The direct type-I and indirect type-II optical transitions between the quantized valence-band and conduction-band states are also drawn.

different subbands are obtained for the lowest AlAs conduction-band states. In structures grown in the [001] direction, the heavy longitudinal mass m_l is the quantization mass for the minima aligned along this growth direction (X_z), whereas the light transversal mass m_t is the quantization mass for the X_x and X_y minima aligned along the [100] and [010] directions, respectively. Thus the lowest confined X sublevel located in the AlAs layer should always be an X_z state.

The lowest-energy band gap of these type-II superlattices is determined by transitions involving the spatially separated Γ valence-band states of the GaAs and the confined X conduction-band states of the AlAs, as schematically depicted in Fig. 1. The respective oscillator strengths of these Γ - X or type-II transitions, however, are very small compared to the direct Γ - Γ or type-I transitions at higher energy because they are indirect in real and in \mathbf{k} space.

With this basic description of the electronic band structure, as derived from the simple Kronig-Penney model, the low-temperature absorption spectra and the main features of the photoluminescence spectra of type-II superlattices can be explained. As an example, Fig. 2 depicts the absorption and photoluminescence (PL) spectra of an (11,24) GaAs/AlAs type-II SPS (with $m = 11$ and $n = 24$) at low temperature. The absorption spectrum shows the direct transitions involving Γ electrons and holes and reveals the $n = 1$ heavy- and light-hole excitons at 1.87 and 1.93 eV, respectively, as well as the $n = 1$ split-off band exciton at 2.21 eV. The absorption coefficient is smaller by orders of magnitude at lower energies, as expected for the indirect type-II transitions.^{10,14} After photoexcitation of electrons and holes in the Γ -related conduction- and valence-band states, some electrons relax down to the lowest confined Γ state of the GaAs layer. Recombination with heavy holes leads to the broad type-I photoluminescence peak in Fig. 2. Peter *et al.*¹⁵ have determined the lifetime of this luminescence to be less than 20 ps. This fast decay is attributed to the real-space

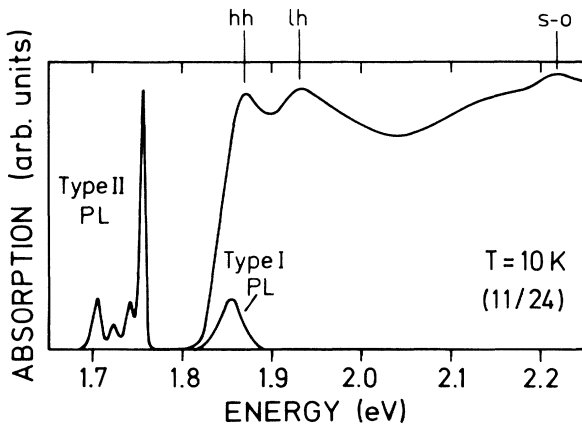


FIG. 2. Low-temperature absorption spectrum of the $(m, n) = (11, 24)$ SPS together with the corresponding PL spectrum (for details see text).

transfer of electrons from the lowest Γ conduction-band state $|\Gamma_1\rangle$ to the energetically lower X -states confined in the adjacent AlAs layers. However, some of the photo-created hot Γ electrons may also scatter to the X -related states before they relax down to the lowest confined Γ state. This competing relaxation channel becomes important if the Γ - X transfer rate and the intravalley relaxation rate are comparable. In Fig. 2, the luminescence features at lower energy correspond to recombination of localized X -point excitons due to the indirect type-II transition.^{9,10,14} Typical radiative lifetimes of the type-II PL are of the order of 10^{-6} sec.^{10,16,17,23}

However, the simple Kronig-Penney model is unable to explain the detailed spectral structure of the type-II luminescence and its variation with the superlattice parameters^{10,14} or with pressure.²⁴ In the envelope-function approximation, it is assumed that the Bloch functions of the different materials are the same, which is not exactly true for the GaAs/AlAs material system. As a consequence, the translational crystal symmetry is destroyed in the superlattice direction z . This leads to mixing of the X_z states in the AlAs with Γ states in the GaAs, induced by an interface potential.^{17,25,26} Γ - X_z mixing can be included in the transfer-matrix approach to the envelope-function approximation,²⁷ as was recently demonstrated by Pulsford *et al.*²⁶ In addition, more sophisticated calculations, such as the tight-binding method,²⁸⁻³⁰ the one-band Wannier-function method,³¹ as well as the pseudo-potential method,^{32,33} take into account all symmetry properties of the superlattice potential. The periodicity of the superlattice potential implies that the three-dimensional Brillouin zone is back folded into the reduced superlattice or mini Brillouin zone. As a further result of these calculations, it turns out that mixing not only takes place between Γ and X_z states but also between X_x and X_y states.^{29,31}

The question which of the AlAs X states are lowest in energy has been discussed in the literature for quite a while.^{9,29,34} The situation becomes even more complicated because energy shifts due to the built-in strain of the AlAs layers must be included. However, recent optically detected magnetic resonance (ODMR) studies by van Kesteren *et al.*³⁵ have definitely shown that in type-II GaAs/AlAs SPS's, the X_z states with the heavier longitudinal mass are lowest, as long as the AlAs thickness is smaller than ≈ 55 Å, corresponding to about 20 monolayers. For AlAs thicknesses exceeding 20 monolayers, however, the $X_{x,y}$ states become lowest, due to the strain-induced lowering of the $X_{x,y}$ valleys with respect to the X_z valley. According to these results, the lowest $X_{x,y}$ states should lie just slightly below the lowest X_z state for the (11,24) type-II GaAs/AlAs SPS.

We now turn to the spectral structure of the type-II luminescence in Fig. 2. The optical matrix element for the type-II Γ - X_z transition involving Γ valence-band states and "mixed" X_z conduction-band states is nonzero only because of the Γ admixture to the X_z states. The strength of the optical transition without participation of a phonon thus is a measure for the Γ - X_z mixing. Since Γ - X_z mixing can be strong in type-II GaAs/AlAs SPS's,

an intense zero-phonon line and much weaker phonon replicas at lower energies are expected for the type-II Γ - X_z luminescence. Mixing of the $X_{x,y}$ and Γ conduction-band states is only possible via potential fluctuations associated with interface roughness, but it turns out to be much less effective than Γ - X_z mixing via the interface potential.^{35,36} As a consequence, the PL spectrum due to type-II Γ - $X_{x,y}$ transitions is dominated by phonon replicas. Keeping in mind that the X_z and $X_{x,y}$ states are almost degenerate for the (11,24) sample, we interpret the main type-II PL peak at higher energy in Fig. 2 as the zero-phonon line of the Γ - X_z transition. The three weaker type-II PL peaks at lower energies are ascribed to the indirect Γ - $X_{x,y}$ transitions with participation of Brillouin-zone boundary TA, LA, and LO phonons of the AlAs layer.¹⁶

We would like to point out that the indirect type-II recombination can be described in a two-step process via an intermediate Γ conduction-band state. Electrons of the lowest-lying X conduction-band states are scattered into virtual conduction-band states at the Γ point, and then recombine with holes of the Γ valence-band states. The scattering is caused by electron-phonon interaction, by potential fluctuations due to interface roughness (Γ - $X_{x,y}$ mixing), and the interface mixing potential (Γ - X_z mixing).³⁷ Consequently, the type-II luminescence spectra may give a hint for the scattering process between Γ - and X -related conduction-band states. However, only the lowest-lying X states contribute to the type-II luminescence, which is different for the Γ - X scattering investigated in this paper. In addition, the type-II luminescence is due to recombination of localized X excitons. We will come back to this point in Sec. V, where we discuss the scattering mechanisms for the real-space Γ - X transfer.

The strength of the indirect type-II luminescence in comparison to the direct type-I luminescence provides strong evidence for an efficient spatial transfer of electrons from the Γ -related states in the GaAs layer to the X -related states in the AlAs layers. In the following, we focus on the experimental investigation of this real-space charge transfer.

III. EXPERIMENTAL RESULTS

We have investigated nine type-II $(\text{GaAs})_m/(\text{AlAs})_n$ SPS's and three type-II $(\text{Al}_x\text{Ga}_{1-x}\text{As})_m/(\text{AlAs})_n$ MQW's. All the samples were grown by molecular-beam epitaxy (MBE) on (001)-oriented substrates. The parameters of the superlattice structures, i.e., the $(m, n; x)$ values, which have been determined independently by double crystal x-ray diffraction, are listed in Table I. The noninteger m and n values are due to interface roughness. The GaAs substrate of all samples was removed by selective chemical etching in order to allow differential transmission spectroscopy.

A. Type-II GaAs/AlAs short-period superlattices

In the case of the all binary GaAs/AlAs SPS's we have determined the Γ - X scattering-time constants by performing nonresonant pump and probe experiments. Optical pulses of 70 fs are generated at 622 nm in a

TABLE I. $(m, n; x)$ values from double-crystal x-ray diffraction together with the experimentally determined Γ - X transfer times τ at $T = 295$ and 10 K.

Sample no.	(m, n)	x	τ (ps)	
			$T = 295$ K	$T = 10$ K
1	(7.6, 7.9)	0	0.12	
2	(8.0, 9.0)	0	0.20	0.17
3	(8.8, 8.8)	0	0.30	0.38
4	(8.8, 42.4)	0	0.36	0.45
5	(10.3, 17.1)	0	0.39	0.40
6	(10.1, 23.5)	0	0.43	0.49
7	(9.7, 37.3)	0	0.50	0.47
8	(11, 24)	0		0.65
9	(12.1, 12.2)	0	0.62	0.87
10	(35.3, 17.7)	0.4		1.9
11	(39.0, 33.5)	0.36	1.9	4.3
12	(68.3, 36.3)	0.37	2.3	22

colliding-pulse mode-locked (CPM) laser using the standard four-prism configuration for intracavity dispersion compensation. The output of this laser is amplified in a six-pass dye flow cell amplifier pumped by a Cu-vapor laser at a repetition rate of 7 kHz. The pulse duration after chirp compensation is 80 fs. After splitting this beam, one beam is used for excitation of the sample, and the other creates the probe continuum in an ethylene-glycol jet. In the first experiments (compare Fig. 3) the continuum exhibited a pronounced chirp of the order of 8 fs/nm for the spectral range from 550 to 730 nm. This chirp now is reduced to 1 fs/nm by removing all glass components in the continuum-beam path. The continuum light transmitted through the sample is dispersed by a grating spectrometer and recorded differentially by an optical multichannel detector. Alternatively, a photomultiplier can be used to record the decay of the photoinduced transmission at a fixed wavelength using lock-in techniques with a chopper synchronized to the 7-kHz pulse train of the pump beam. The latter method provides an improvement of the signal-to-noise ratio by a factor of 10. The energy- and time-resolved differential transmission spectrum (DTS) $\Delta T/T_0$ at $T = 10$ K is plotted in Fig. 3(a) for the (11,24) SPS (sample no. 8). We find a pronounced bleaching of the type-I heavy- and light-hole excitonic transitions for positive time delay between pump and probe pulse, similar to the results for a type-I quantum well obtained by Knox *et al.*³⁸ The bleaching arises from (i) state filling of the Γ -related conduction- and valence-band single-particle states, which build up the exciton state, (ii) screening of the Coulomb interaction between electrons and holes by the photocreated carriers, and (iii) band-gap renormalization via exchange and correlation interaction of the carriers.^{38,39} We also observe a bleaching of the splitoff excitonic transition.⁴⁰ As indicated in Fig. 3(b), holes cannot be excited in the splitoff band by the pump laser with 2-eV photon energy. Thus the contribution to the bleaching signal at 2.21 eV for the splitoff-band excitonic transition due to state filling can only originate from electrons in the lowest Γ state confined in the GaAs.

The temporal evolution of the bleaching signals of the respective excitonic transition is depicted in Fig. 4(a). Each curve is characterized by an initial partial decay down to a quasiconstant value, which is different for the three excitonic transitions. No further appreciable change of the DTS signals is observed up to 20 ps, which is the upper limit for the Γ - X transfer time in GaAs/AlAs SPS.¹⁵ This initial fast decay at the lowest excitonic transition is not present in either bulk samples of GaAs or $\text{Al}_x\text{Ga}_{1-x}\text{As}$,⁴¹ or in type-I quantum wells.³⁸ Apparently, the initial recovery of the bleached absorption has to be attributed to reduction of state filling due to scattering of electrons from the Γ conduction-band states of the GaAs to the X -like states of the AlAs. In addition, a reduced contribution to screening is expected for the scattered electrons, since they are confined in the spatially separated AlAs layers. Consequently, the Γ - X transfer of electrons is directly monitored by the DTS signal of the split-off-band exciton, whereas the temporal evolution of the heavy- and light-hole exciton signal is also influenced by relaxation of hot photogenerated holes down to the heavy-hole valence-band edge. The remaining signal is attributed to state filling of the still-occupied hole states of the Γ valence band in GaAs and also to screening of the excitonic enhancement by holes in the GaAs and electrons in the AlAs. We determine a Γ - X transfer time of 0.65 ps for the (11,24) SPS, shown in

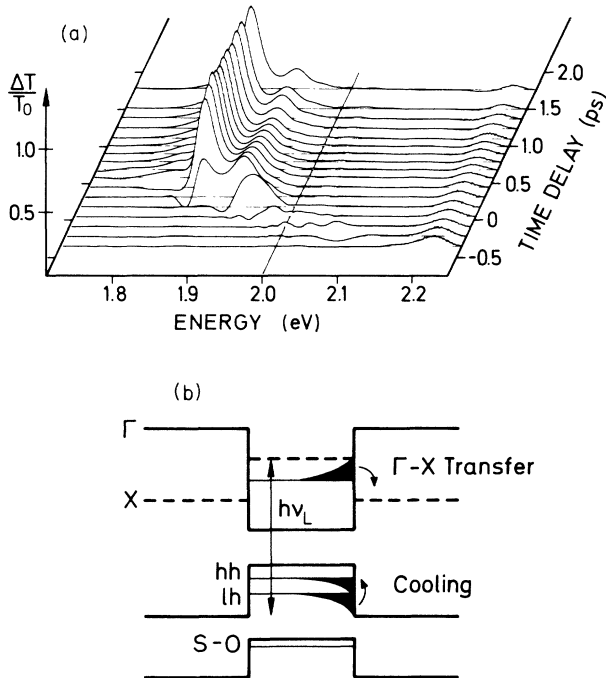


FIG. 3. Energy- and time-resolved differential transmission spectrum (DTS) of the $(m,n)=(11,24)$ SPS at $T=10$ K. In this experiment a pronounced chirp of the continuum of 8 fs/nm is observed. The time delay is chosen to be zero for the pump-laser energy of 2 eV. In the lower part the induced hot carriers are visualized, and the Γ - X transfer of electrons, as well as the cooling of holes are indicated by the arrows.

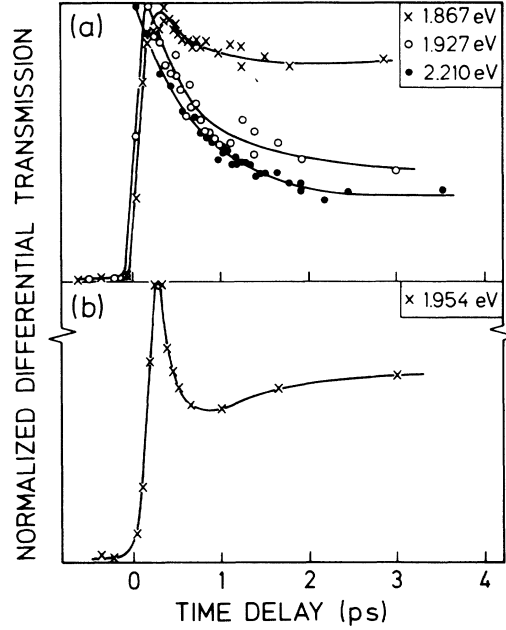


FIG. 4. Temporal courses of the DTS signal at the heavy-hole, light-hole, and split-off-band excitonic transitions for the $(m,n)=(11,24)$ SPS in the upper part and at the heavy-hole excitonic transition for the $(m,n)=(8,9)$ SPS in the lower part.

Figs. 3 and 4(a).

The time dependence of the DTS signal at the heavy-hole excitonic transition of an (8,9) SPS is depicted in Fig. 4(b). The Γ - X transfer is much faster in this SPS, with a time constant of about 0.17 ps. Due to this fast partial recovery of the bleached absorption, the subsequent cooling of hot holes down to the heavy-hole band edge can be observed for this sample: The DTS signal increases again with a time constant of the order of 1 ps, reflecting the increase of state filling of the lower-energy states due to cooling of the holes.

We have investigated seven more $(\text{GaAs})_m/(\text{AlAs})_n$ SPS's with different (m,n) values, as listed in Table I, in order to determine in more detail the dependence of the Γ - X transfer time constants on the individual GaAs and AlAs layer thicknesses. The low-temperature experimental values for the Γ - X transfer time constants are listed in Table I. The relative uncertainty of these data is estimated to be less than 15%.

The experimental values for the Γ - X scattering time constants versus the number m of monolayers of GaAs are plotted in Fig. 5. We find a pronounced and continuous increase of the Γ - X transfer times with increasing GaAs layer thickness, whereas the Γ - X transfer times are almost independent of the AlAs layer thickness. For instance, the number m of monolayers of GaAs for sample nos. 3 and 4 as well as for sample nos. 5, 6, and 7 is almost the same, whereas the AlAs layer thickness varies by more than a factor of 4 or 2, respectively. However, in both cases, the Γ - X transfer times are comparable.

We thus conclude from our experimental results that

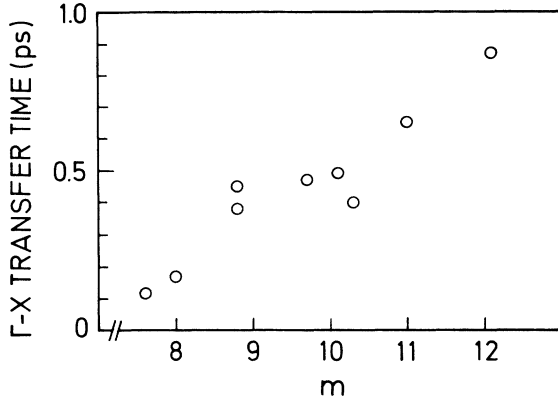


FIG. 5. Experimentally determined time constants for the Γ - X transfer at $T=10$ K vs the number m of monolayers of GaAs (obtained by double crystal x-ray diffraction).

the Γ - X transfer rate is mainly determined by the GaAs and scarcely by the AlAs layer thickness.

B. Type-II $\text{Al}_x\text{Ga}_{1-x}\text{As}/\text{AlAs}$ multiple quantum wells

An investigation of the dependence of the Γ - X transfer time on the number m of monolayers of GaAs is restricted in the all binary system to $m \leq 12$, because for $m > 12$ the character of the SPS changes to type I. However, type-II behavior can be maintained for much thicker layers if the GaAs is replaced by $\text{Al}_x\text{Ga}_{1-x}\text{As}$, provided x is chosen properly. We therefore have investigated three type-II $\text{Al}_x\text{Ga}_{1-x}\text{As}/\text{AlAs}$ MQW's. At low temperature these samples could not be excited with the CPM laser, because the direct Γ - Γ band gap is larger than 2 eV. We therefore have performed pump and probe experiments using a cavity-dumped hybridly mode-locked dye laser with the ability to tune the laser emission wavelength.⁴² This experimental setup provides a time resolution of about 1 ps. The laser wavelength was tuned to excite and probe resonantly "direct" heavy-hole (hh) excitons for each sample.

The temporal evolution of the bleaching at the hh excitonic transition is depicted in Fig. 6 for all three samples at $T=10$ K. We again observe in all cases an initial partial recovery of the bleached absorption, with different time constants for the three different samples. The initial decrease of the bleaching signal now can be attributed solely to the Γ - X transfer of electrons, because cooling of hot carriers within the Γ states does not contribute in the case of resonant excitation. Similar to the case of type-II GaAs/AlAs SPS's, no further appreciable change in the bleaching signal occurs after the initial partial recovery up to 300 ps due to the long lifetime of "indirect" X excitons. We can exclude any coherent effects⁴³ in these pump and probe experiments with perpendicularly polarized beams because the initial decay of the bleaching signal is resolved in each case. In addition, we have checked using self-diffraction experiments⁴⁴ that the dephasing times T_2 are always shorter than the time resolution of

our experiment under the present conditions.

The important result of the data in Fig. 6 is that the Γ - X transfer rates are now in the picosecond regime and increase from 1.9 ps for $m=35.5$ (sample no. 10) up to 22 ps for $m=68.3$ (sample no. 12).

We can verify these results by applying an independent time-resolved technique. Transient ps-luminescence experiments using a synchroscan streak-camera system provide a time resolution of about 15 ps (for details of the experimental setup see Ref. 15). The luminescence spectra of the type-II $\text{Al}_x\text{Ga}_{1-x}\text{As}/\text{AlAs}$ samples only exhibit one photoluminescence peak due to recombination of the direct $n=1$ heavy-hole exciton. Luminescence due to type-II transitions is absent probably because the spatial separation of electrons in the X conduction-band states of the AlAs and holes in the Γ valence-band states of the $\text{Al}_x\text{Ga}_{1-x}\text{As}$ is too large. The time-resolved PL spectra of the type-I luminescence for the ($m=39$, $n=33.5$; $x=0.36$) sample and the ($m=68.3$, $n=36.3$; $x=0.37$) sample are depicted in Fig. 7. The decay of this luminescence directly monitors the disappearance of electrons from the lowest Γ state to the X states in the neighboring AlAs layers. As expected from Fig. 6(b), the fast transfer time of 4.3 ps for the ($m=39$, $n=33.5$; $x=0.36$) MQW cannot be resolved. However, the decay of the

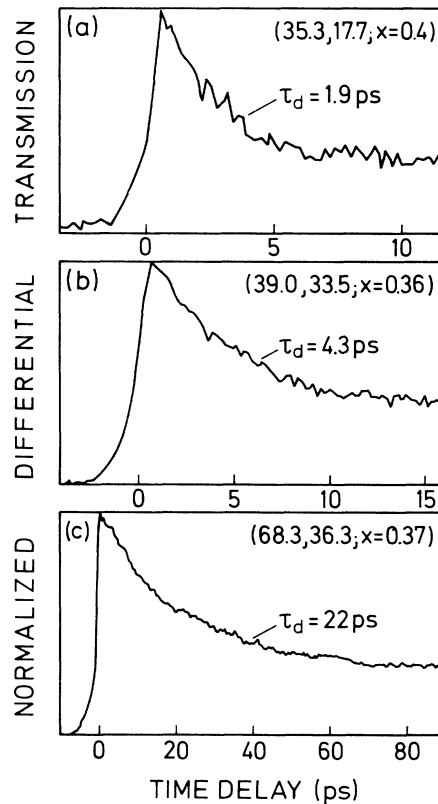


FIG. 6. Temporal courses of the heavy-hole exciton bleaching for three different $\text{Al}_x\text{Ga}_{1-x}\text{As}/\text{AlAs}$ MQW's at low temperature, obtained by applying the resonant pump and probe method.

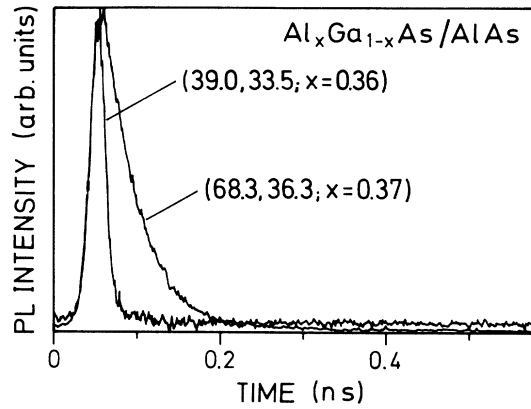


FIG. 7. Time-resolved spectra of the type-I photoluminescence for sample nos. 11 and 12 at $T = 10$ K.

type-I luminescence is clearly resolved in the case of the ($m = 68.3, n = 36.3; x = 0.37$) MQW, and a decay time of about 36 ps is derived from a semilogarithmic plot. The repetition rate of the laser pulses in the luminescence experiment was 76 MHz, compared to 500 kHz in the pump and probe experiment. Thus, in the luminescence experiment, the electrons accumulate in the X states of the AIAs, since the lifetime of the X electrons typically is in the order of 10^{-6} s. Consequently, fewer final unoccupied X states are available for the Γ - X transfer of electrons photocreated in the Γ states by each laser pulse. This may explain the larger time constant of 36 ps obtained in the luminescence experiment compared to 22 ps determined by the pump and probe experiment with 500-kHz repetition rate. In addition, the type-I luminescence exhibits a Stokes shift of 6 meV in respect to the direct heavy-hole absorption peak, which is due to localization of heavy-hole excitons. The Γ - X transfer time, determined by time-resolved luminescence, may be longer due to this localization.

From the experimental data, we conclude that the Γ - X scattering times are strongly dependent on the GaAs and $\text{Al}_x\text{Ga}_{1-x}\text{As}$ layer thickness, but the scattering times do not show a significant dependence on the thickness of the AIAs layers. The scattering times increase with increasing thickness from about 100 fs in a $(\text{GaAs})_m/(\text{AlAs})_n$ type-II SPS with $m = 7.6$ up to 22 ps in an $(\text{Al}_x\text{Ga}_{1-x}\text{As})_m/(\text{AlAs})_n$ type-II MQW with $m = 68.3$.

IV. DISCUSSION

We now turn to a discussion of the experimental data presented in the preceding sections. In order to explain the relative importance of the (Al,Ga)As and AIAs layer thicknesses and to calculate the respective Γ - X transition rates we have to apply Fermi's "golden rule." The transfer rate τ^{-1} from the lowest confined Γ state $|\Gamma_1\rangle$ to all final X states of the AIAs layer is proportional to the sum over all squared matrix elements:

$$\tau^{-1} \propto \sum_{\substack{\text{final} \\ X \text{ states}}} |\langle \psi_1^\Gamma | H_{sc} | \psi^X \rangle|^2. \quad (1)$$

The quantitative evaluation of the matrix elements requires knowledge of the orthogonal ψ_1^Γ and ψ^X envelope wave functions and, in addition, the scattering mechanism that determines the perturbation Hamiltonian H_{sc} .

Due to the staggered band alignment, the confined X envelope wave functions ψ^X are mainly located in the AIAs layers, whereas the Γ envelope wave function ψ_1^Γ is mainly located in the (Al,Ga)As layers. It is evident that this spatial separation of the Γ and X envelope wave functions diminishes the matrix elements in Eq. (1), which determine the Γ - X transfer rate.

The simple Kronig-Penney model, as described in Sec. II, provides Γ and X envelope wave functions $\varphi_i^\Gamma(z)$ and $\varphi_i^X(z)$ (i indicates the number of the sublevel), which are not orthogonal. Consequently, the overlap integral $\langle \varphi_1^\Gamma | \varphi_1^X \rangle$ is nonzero, and represents a measure of the spatial separation of the Γ and X wave functions. This is illustrated in Figs. 8(a) and 8(b) for a (28,8; $x = 0.28$) type-II superlattice. For this superlattice structure only one X sublevel, namely the lowest X_z sublevel, lies energetically below the $|\Gamma_1\rangle$ state. In Fig. 8(a) the Kronig-Penney envelope wave functions φ_1^Γ and $\varphi_1^{X_z}$ are plotted versus λ , the spatial coordinate characterized by the number of the respective monolayer in the z direction. φ_1^Γ and $\varphi_1^{X_z}$ are

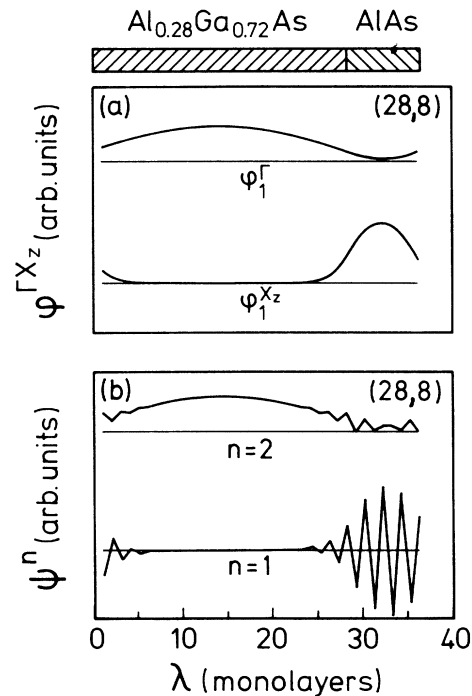


FIG. 8. Envelope wave functions for a type-II ($m = 28, n = 8; x = 0.28$) superlattice obtained (a) by simple Kronig-Penney model calculations (Ref. 22) and (b) by one-band Wannier-orbital calculations (taken from Ref. 31) for the bottom ($q = 0$) of the two lowest-lying minibands. The nonorthogonal Kronig-Penney envelope wave functions $\varphi_1^{X_z}$ and φ_1^Γ in (a) correspond to the orthogonal envelope wave functions ψ^1 and ψ^2 in (b), respectively.

calculated for the bottom of the respective minibands ($q=0$).²² For comparison, the wave functions $\psi^1(\lambda)$ and $\psi^2(\lambda)$ plotted in Fig. 8(b) represent orthogonal and more realistic envelope wave functions obtained for the same superlattice structure by the one-band Wannier-function method (taken from Ref. 31). $\psi^1(\lambda)$ and $\psi^2(\lambda)$ of Fig. 8(b) are also calculated for $q=0$ (Ref. 31) and correspond to the Kronig-Penney envelope wave functions $\varphi_1^{X_z}(\lambda)$ and $\varphi_1^\Gamma(\lambda)$ of Fig. 8(a), respectively. The strong oscillations of $\psi^1(\lambda)$ in Fig. 8(b) originate from the large k wave vector of the X_z state in bulk AlAs and ensure that the envelope wave functions $\psi^1(\lambda)$ and $\psi^2(\lambda)$ are orthogonal. A comparison of Figs. 8(a) and 8(b) shows that the Kronig-Penney envelope wave functions in fact account fairly well for the spatial separation. In the following, we thus take the overlap integrals $\langle \varphi_1^\Gamma | \varphi_i^X \rangle$ as a quantity for the spatial separation of the Γ and X wave functions.

To get a first insight into the effect of the spatial separation on the Γ - X scattering time constants, we replace the matrix elements $|\langle \psi_1^\Gamma | H_{sc} | \psi^X \rangle|$ merely by the spatial overlap integrals $\langle \varphi_1^\Gamma | \varphi_i^X \rangle$. We additionally assume that the scattering is elastic, which is true for the type-II GaAs/AlAs SPS, as will be shown in Sec. V. The summation in Eq. (1) then simply must be taken over all X_i subbands lying energetically below the $|\Gamma_1\rangle$ state, because the two-dimensional density of states is constant for each X_i subband. The Γ - X transfer rate then can simply be written

$$\tau^{-1} \propto S_{X_z} + 2\sqrt{m_l/m_t} S_{X_x}, \quad (2)$$

where m_l and m_t are, respectively, the longitudinal and transverse effective masses of the X valley in the bulk AlAs. S_{X_z} and S_{X_x} are sums over squared overlap integrals:

$$S_{X_z} = \sum_i |\langle \varphi_1^\Gamma | \varphi_i^{X_z} \rangle|^2, \quad (3)$$

$$S_{X_x} = \sum_i |\langle \varphi_1^\Gamma | \varphi_i^{X_x} \rangle|^2.$$

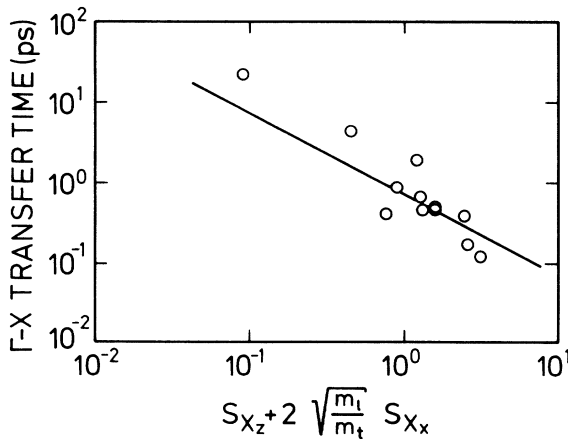


FIG. 9. Plot of the experimentally determined Γ - X transfer times vs the calculated sums over squared overlap integrals according to Eq. (2) for all studied type-II samples. The line indicates the expected relationship according to Eq. (2).

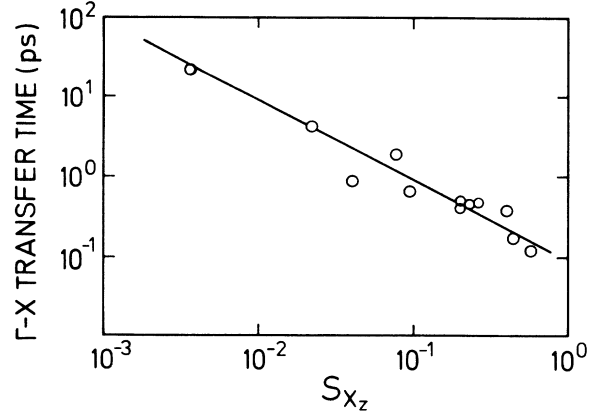


FIG. 10. Plot of the experimentally determined Γ - X transfer times vs S_{X_z} for all studied type-II samples. The line indicates the expected linear relationship.

The factor $2\sqrt{m_l/m_t} = 4.7$ takes into consideration the different densities of final states for scattering into the X_z states as compared to scattering into the $X_{x,y}$ states. In Fig. 9 the experimental time constants τ are plotted versus the right-hand expression of Eq. (2) calculated for the respective samples. The envelope wave functions are calculated as described in Ref. 22. The expected linear relation according to Eq. (2) is indicated by the line, representing a slope of 1 in this double logarithmic plot.

In Sec. V it will be discussed that the scattering of Γ electrons may predominantly occur into the X_z states, if strong Γ - X_z mixing is present. For this reason, we have also plotted in Fig. 10 the experimental time constants τ versus the sum S_{X_z} of squared overlap integrals, taking into account only the $\varphi_i^{X_z}$ envelope wave functions. The solid line again indicates a linear dependence.

Figures 9 and 10 indicate that the experimental data are already fairly well described, taking into account only the envelope wave function overlap. This agrees with our interpretation that the Γ - X transfer rate is mainly determined by the spatial overlap of the Γ and X wave functions. However, even though Fig. 10 seems to provide a better fit, the approximations made are too crude to definitely conclude that scattering preferably involves X_z states.

An interesting consequence of our calculations is that we are not only able to explain the pronounced dependence of Γ - X transfer times on the (Al,Ga)As layer thickness, but also that the Γ - X scattering times are almost independent of AlAs layer thickness. In fact, the overlap of the Γ_1 and X_i wave functions corresponding to a particular subband i decreases with increasing (Al,Ga)As or AlAs layer thickness. However, in the case of increasing AlAs layer thickness, the decreasing overlap is at least partly compensated by the increasing number of X subbands lying below the Γ_1 state.

V. THE SCATTERING MECHANISM(S)

In bulk GaAs the Γ - X intervalley scattering is due to electron-LO-phonon deformation-potential interac-

tion.^{45–47} Only longitudinal-optical phonons cause the Γ - X intervalley scattering because of selection rules due to the crystal symmetry.⁴⁶ The contribution of LO-phonon polar-optical scattering is unimportant for the Γ - X scattering because of the strong decrease of the Fröhlich interaction with increasing phonon wave vector q_{ph} .

However, the real-space Γ - X transfer in a type-II superlattice is different in several respects from Γ - X intervalley scattering in bulk material. Firstly, the Γ and X states of a type-II superlattice are confined in different layers; i.e., the respective wave functions are spatially separated [Figs. 8(a) and 8(b)]. Secondly, the spatial transfer of electrons induces an electric field between the (Al,Ga)As and AlAs layers, resulting in a shift of the Γ and X eigenenergies.⁴⁸ Finally, additional scattering due to potential fluctuations caused by interface roughness (Γ - $X_{x,y}$ mixing) and due to the interface mixing potential (Γ - X_z mixing) is possible in type-II (Al,Ga)As/AlAs superlattices, in contrast to bulk semiconductors.

As already mentioned in Sec. II, the luminescence spectra of type-II (GaAs)_{*m*}/(AlAs)_{*n*} SPS's may give a hint for the strength of different scattering mechanisms causing the real-space Γ - X transfer. If the X_z state is lowest, strong Γ - X_z mixing via the interface mixing potential leads to an intense zero-phonon line for type-II (GaAs)_{*m*}/(AlAs)_{*n*} SPS's. Consequently, scattering of Γ electrons into the X_z states, caused by the interface mixing potential, could dominate in type-II (GaAs)_{*m*}/(AlAs)_{*n*} SPS's.⁴⁹ This statement might not hold for the type-II Al_{*x*}Ga_{1-*x*}As/AlAs MQW samples, because type-II luminescence has not been observed for these samples. In the remaining part of this paper we present and discuss the dependence of the Γ - X transfer times on carrier density and lattice temperature for all the samples. This provides insight into the nature of the underlying scattering process.

We have performed intensity- and temperature-dependent measurements of the Γ - X time constants. The initially induced carrier density N_{exc} was varied between 1×10^{12} and 1×10^{13} cm⁻² in the case of the nonresonant pump and probe experiments for type-II GaAs/AlAs SPS's. In the resonant pump and probe experiments of the type-II Al_{*x*}Ga_{1-*x*}As/AlAs MQW, the carrier density N_{exc} was varied between 1×10^{10} and 5×10^{12} cm⁻². In both cases, however, the Γ - X transfer times derived from the initial partial recovery of the bleached absorption do not change within the limits of the experimental accuracy. This is illustrated in Fig. 11 for sample no. 12, where the temporal evolution of the DTS at the heavy-hole exciton is shown for $N_{exc} = 1 \times 10^{10}$ cm⁻² and $N_{exc} = 5 \times 10^{11}$ cm⁻². We can thus rule out electron-carrier scattering as the underlying process for the Γ - X transfer.

We now consider the results of the temperature dependence of the Γ - X scattering time constants obtained by resonant pump and probe experiments. The temporal evolution of the DTS signal for two type-II Al_{*x*}Ga_{1-*x*}As/AlAs MQW's at room temperature is shown in Fig. 12. Qualitatively, the temporal traces are comparable to the low-temperature results of Fig. 6.

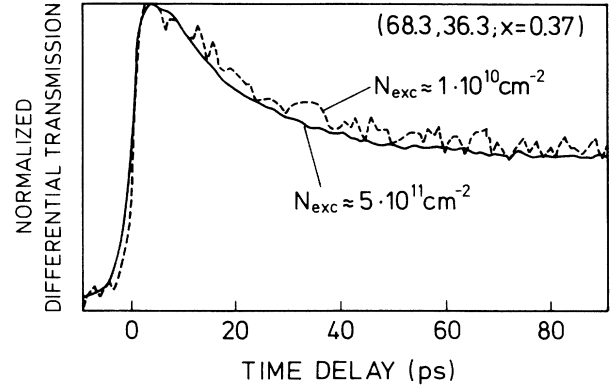


FIG. 11. Temporal courses of the heavy-hole exciton bleaching for sample no. 12 for different initial carrier densities N_{exc} , obtained by applying the resonant pump and probe method.

However, the initial decay of 1.9 ps for the ($m = 39, n = 33.5; x = 0.36$) MQW [Fig. 12(a)] is faster than at low temperature [4.3 ps; cf. Fig. 6(b)]. This difference between room temperature and low temperature is even more pronounced in case of the ($m = 68.3, n = 36.3; x = 0.37$) MQW [Fig. 12(b)] with transfer times of 2.5 and 22 ps at 300 and 10 K, respectively. The experimentally determined decay times (solid points) of the bleaching signal are plotted for the ($m = 39, n = 33.5; x = 0.36$) and the ($m = 68.3, n = 36.3;$

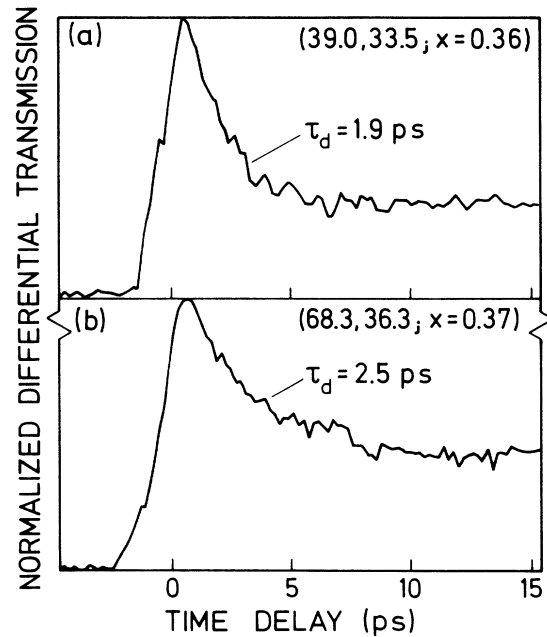


FIG. 12. Temporal courses of the heavy-hole exciton bleaching for sample nos. 11 and 12 at room temperature, obtained by applying the resonant pump and probe method.

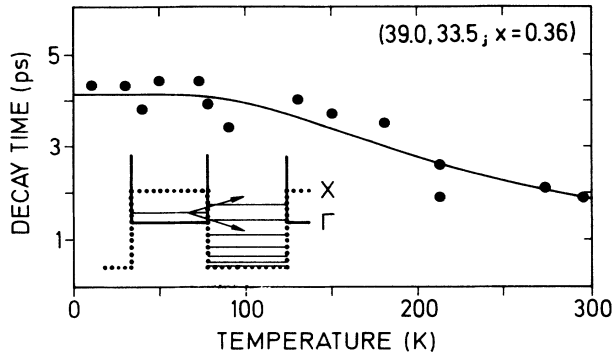


FIG. 13. Experimentally determined Γ - X transfer times vs crystal temperature for the ($m=39, n=33.5; x=0.36$) MQW. The solid curve represents the theoretically expected temperature dependence according to Eq. (4) for $J_{\text{abs}}/J_{\text{em}}=3.3$. The arrows illustrate the Γ - X transfer of an electron by absorption or emission of an LO phonon ($h\nu_{\text{ph}}=39$ meV), respectively.

$x=0.37$) MQW's for the entire range from $T=10$ K up to 295 K in Figs. 13 and 14, respectively.

For the interpretation of this data we must consider that exciton ionization at higher temperatures may also cause an initial recovery of the bleached absorption. Knox *et al.*⁵⁰ determined the time constant for ionization of heavy-hole excitons in type-I quantum wells to be 300 fs at room temperature. We thus assume that thermalization of resonantly excited cold electrons within the Γ states of the type-II $\text{Al}_x\text{Ga}_{1-x}\text{As}/\text{AlAs}$ MQW also occurs on a subpicosecond time scale at room temperature. Consequently, the picosecond recovery of the bleached absorption in Fig. 12 can be attributed to the real-space Γ - X transfer of thermalized Γ electrons. We

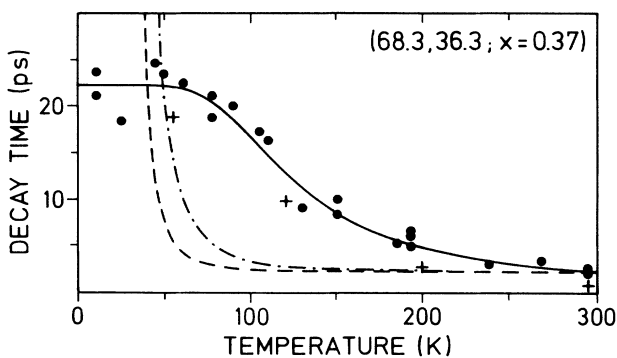


FIG. 14. Experimentally determined Γ - X transfer times vs crystal temperature for the ($m=68.3, n=36.3; x=0.37$) MQW obtained by resonant (circles) and nonresonant (crosses) pump and probe experiments. The solid curve represents the theoretically expected temperature dependence according to Eq. (4) for $J_{\text{abs}}/J_{\text{em}}=31$. The dashed and dashed-dotted curves are obtained for ionized impurity scattering assuming a carbon impurity concentration of $N_{\text{imp}}=10^{10}$ cm^{-2} and $N_{\text{imp}}=10^{11}$ cm^{-2} , respectively.

can experimentally verify that the initial decay of the bleaching signal in the resonant pump and probe experiments is due to the Γ - X transfer and not due to exciton ionization for all temperatures. We have performed non-resonant pump and probe experiments at higher temperatures for the ($m=68.3; n=36.3; x=0.37$) type-II sample. We again find an initial partial decay of the heavy-hole bleaching signal, which now can be unambiguously attributed to the Γ - X transfer of Γ electrons, as already discussed in Sec. III. The time constants obtained from the initial recovery are plotted as crosses in Fig. 14. The experimentally found Γ - X transfer time constants again exhibit a pronounced decrease with increasing temperature, as in the case of the resonant pump and probe experiments. The time constants obtained by the non-resonant pump and probe experiments lie slightly below the values determined in the resonant pump and probe experiments. In the nonresonant case, electrons are photoexcited in energetically higher Γ states. Since the spatial overlap of Γ and X envelope wave functions increases with increasing energy due to a greater delocalization, the Γ - X transfer rate of hot Γ electrons is faster than for resonantly excited Γ electrons.

In order to find an explanation for the observed decrease of the Γ - X transfer time constants with increasing temperature, we discuss in the following different scattering mechanisms with regard to their temperature dependence. However, it is important to keep in mind that a change of the electron distribution function $f(E, T)$ has to be considered in the case of energy-dependent scattering rates τ^{-1} , in addition to an explicit temperature dependence of τ^{-1} in Eq. (1).

In two-dimensional systems, interface scattering and also alloy scattering explicitly depend neither on the lattice temperature T nor on electron energy E .⁵¹⁻⁵⁴ We thus rule out interface as well as alloy scattering to be the most efficient Γ - X scattering mechanisms for the $\text{Al}_x\text{Ga}_{1-x}\text{As}/\text{AlAs}$ type-II samples depicted in Figs. 13 and 14. Alternatively, a qualitatively similar trend, namely an increase of the scattering rate τ^{-1} with increasing temperature, is predicted for ionized impurity scattering as well as electron phonon scattering.^{45,55,56} The ionized impurity scattering rate τ_{ion}^{-1} is proportional to the concentration N_{ion} of ionized impurities,^{45,55} which implies an explicit temperature dependence. Recently, Ferreira *et al.*⁵⁷ have demonstrated that impurity-induced intersubband scattering rates in type-I $\text{GaAs}/\text{Al}_x\text{Ga}_{1-x}\text{As}$ quantum wells with $N_{\text{ion}}=10^{10}$ cm^{-2} are about 2 orders of magnitude smaller than phonon-assisted processes. Since in our intentionally undoped samples the impurity concentration N_{imp} is unlikely to be more than 10^{10} cm^{-2} , we do not expect ionized impurity scattering to be important. In addition, the experimentally found temperature dependence of the time constants cannot be fitted with $N_{\text{ion}}(T)$. This is demonstrated in Fig. 14 by the dashed ($N_{\text{imp}}=10^{10}$ cm^{-2}) and dashed-dotted ($N_{\text{imp}}=10^{11}$ cm^{-2}) curves, which represent calculations of the ionized impurity scattering for an impurity with $E_b=37$ meV [carbon acceptor for $x=0.37$ (Ref. 58)]. The calculated curves have been normalized to the experimental room-temperature value. This

disagreement becomes even worse if the linear increase of τ_{ion} with increasing energy E as valid for two-dimensional systems⁵⁵ is taken into account.

We now discuss electron-phonon interaction $H_{e\text{-ph}}$ as the cause of the temperature dependence of the Γ - X transfer times in the type-II $\text{Al}_x\text{Ga}_{1-x}\text{As}/\text{AlAs}$ MQW. The matrix elements $\langle \psi_1^r | H_{e\text{-ph}} | \psi^X \rangle$ in Eq. (1) only contribute for large phonon wave vectors q_{ph} . This is due to the strong oscillations of the X envelope wave functions, in contrast to the Γ envelope wave functions, as illustrated in Fig. 8(b) for an X_2 state. Thus the situation is comparable to bulk GaAs. We can thus assume LO-phonon deformation-potential interaction to cause the Γ - X scattering for this case. Similar to the calculations for intersubband scattering in type-I quantum wells,⁵⁶ we write for the Γ - X transfer rate in the type-II superlattices

$$\tau^{-1} \propto J_{\text{abs}} N_{\text{ph}} + J_{\text{em}} (N_{\text{ph}} + 1), \quad (4)$$

with the phonon occupation probability

$$N_{\text{ph}} = [\exp(h\nu_{\text{ph}}/kT) - 1]^{-1}. \quad (5)$$

The first and second terms of Eq. (4) account for absorption and emission of a phonon with energy $h\nu_{\text{ph}}$, respectively. J_{abs} and J_{em} represent sums over squared matrix elements for phonon absorption and emission. An explicit energy dependence does not occur in Eq. (4), contrary to the case of bulk semiconductors, since the two-dimensional density of states is constant. The temperature dependence of the mean Γ - X scattering time of thermalized Γ electrons is only due to the phonon occupation probability N_{ph} . The effective LO-phonon energy for $\text{Al}_{0.36}\text{Ga}_{0.64}\text{As}$ amounts to $h\nu_{\text{ph}} = 39$ meV.⁵⁹ Normalizing Eq. (4) to $\tau = 1.9$ ps for $T = 295$ K, and taking $J_{\text{abs}}/J_{\text{em}} = 3.3$, we get the solid curve drawn in Fig. 13, which is in good agreement with the experimental data. We can also estimate the fitting parameter $J_{\text{abs}}/J_{\text{em}}$ by replacing J_{abs} and J_{em} by sums over envelope function overlap integrals, as already discussed in Sec. IV:

$$J_{\text{abs, em}} = (S_{X_z})_{\text{abs, em}} + 2\sqrt{m_1/m_t} (S_{X_x})_{\text{abs, em}}. \quad (6)$$

In order to obtain S_{X_z} and S_{X_x} for phonon absorption and phonon emission, the summation in Eq. (3) runs over all X sublevels to which scattering from $|\Gamma_1\rangle$ by, respectively, absorption or emission, of an LO phonon is possible. This is illustrated in the inset of Fig. 13. The Kronig-Penney band-structure calculations provide $J_{\text{abs}}/J_{\text{em}} = 4.3$ for the ($m = 39, n = 33.5; x = 0.36$) MQW, in good agreement with the value $J_{\text{abs}}/J_{\text{em}} = 3.3$ obtained from the fit in Fig. 13. This further supports our conclusion that the underlying Γ - X scattering mechanism is electron-LO-phonon interaction for this type-II sample.

For the ($m = 68.3, n = 36.3; x = 0.37$) MQW (Fig. 14) the alloy composition is close to the direct-indirect crossover.^{59,60} Consequently, the highest-possible final X states for Γ - X transfer by absorption of a phonon are close to the X barrier, and are already strongly delocalized. This leads to a much larger value of $J_{\text{abs}}/J_{\text{em}}$, as compared to the ($m = 39, n = 33.5; x = 0.36$) MQW, and consequently to a more pronounced temperature dependence of the

Γ - X transfer times for this type-II sample. In Fig. 14, $J_{\text{abs}}/J_{\text{em}} = 31$ is needed as a fitting parameter to obtain the solid curve for $\tau(T)$, according to Eq. (4). A comparison of the fitting parameter $J_{\text{abs}}/J_{\text{em}}$ with an estimate according to Eq. (6) is not possible for this type-II sample, because the calculation of $J_{\text{abs}}/J_{\text{em}}$ is too critical in the vicinity of the direct-indirect crossover. Nevertheless, the form of $\tau(T)$ according to Eq. (4), which reflects the freezing out of LO phonons due to the Bose-Einstein distribution N_{ph} , describes the experimental data very well. We therefore conclude that the Γ - X transfer of electrons in these type-II $\text{Al}_x\text{Ga}_{1-x}\text{As}/\text{AlAs}$ MQW's with relatively thick layers of the $\text{Al}_x\text{Ga}_{1-x}\text{As}$ is due to electron-LO-phonon interaction.

Room-temperature measurements of the Γ - X transfer times for the all binary type-II GaAs/AlAs SPS's have also been performed. In Fig. 15 the respective temporal traces of $\Delta T/T_0$ at the splitoff excitonic transitions for an ($m = 8.8, n = 42.4$) and an ($m = 10.3, n = 17.1$) SPS (sample nos. 4 and 5) are depicted for $T = 10$ K (solid curve) and $T = 295$ K (dashed curve). Obviously, the initial partial recovery of the bleached absorption and hence the transfer time constants are independent of temperature. The room-temperature data for the transfer times are listed in Table I together with the low-temperature values for seven type-II GaAs/AlAs SPS's.

Contrary to the experimental results for the thick $\text{Al}_x\text{Ga}_{1-x}\text{As}/\text{AlAs}$ MQW, the freezing out of LO phonons with decreasing temperature does not influence the Γ - X transfer times in the case of the type-II GaAs/AlAs SPS with thin GaAs layers. Consequently, a different, temperature-independent scattering mechanism is dominant in the case of the type-II GaAs/AlAs SPS. We as-

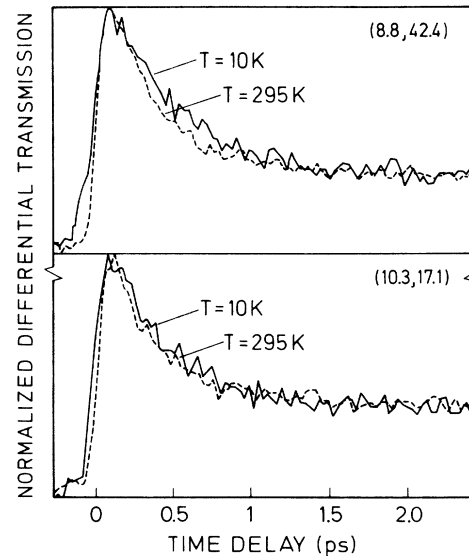


FIG. 15. Time-resolved DTS signals for the ($m = 8.8, n = 42.4$) and ($m = 10.3, n = 17.1$) SPS's at the respective split-off-band excitonic transitions for $T = 10$ and 295 K, obtained by applying nonresonant pump and probe experiments.

sume that interface scattering caused by the interface mixing potential (Γ - X_z mixing) and/or caused by the potential fluctuations due to interface roughness (Γ - $X_{x,y}$ mixing) dominates the Γ - X transfer in the type-II GaAs/AlAs SPS, consisting of thin GaAs layers ($m \leq 12$). These mechanisms are expected to decrease with increasing well width in accordance with the decrease of the probability amplitude of the electron wave function at the interface. Consistently, electron-phonon scattering becomes the dominant scattering mechanism for thick $\text{Al}_x\text{Ga}_{1-x}\text{As}$ layers ($m > 35$).

VI. CONCLUSIONS

The real-space Γ - X transfer of electrons in type-II GaAs/AlAs SPS's and $\text{Al}_x\text{Ga}_{1-x}\text{As}/\text{AlAs}$ MQW's has been studied in detail. The associated time constants have been determined by optical pump and probe experiments. The Γ - X transfer time constants cover a wide range from about 0.1 ps up to about 20 ps, depending on the structural parameters of the SPS. We have demonstrated that the Γ - X scattering rates are essentially determined by the spatial overlap of the initial- and final-state wave functions. As a consequence, the Γ - X transfer time constants show a pronounced increase with increasing thickness of, respectively, the GaAs or $\text{Al}_x\text{Ga}_{1-x}\text{As}$ layers, which confine the Γ states. In contrast, the transfer times are almost independent of AlAs layer thickness, due to the fact that the reduction of wave function overlap for a particular X sublevel with increasing layer thickness is compensated by an increase in the number of X sublevels taking part in the scattering. We have also considered the scattering mechanisms for this real-space charge transfer by measuring the time constants for different induced carrier densities and at different temper-

atures. We have identified electron-LO-phonon interaction as the dominant mechanism due to the decrease of the transfer rate with decreasing temperature for the type-II $(\text{Al}_x\text{Ga}_{1-x}\text{As})_m/(\text{AlAs})_n$ MQW with thick $\text{Al}_x\text{Ga}_{1-x}\text{As}$ layers ($m > 35$). No temperature dependence of the transfer time constants is found in the case of the all binary type-II GaAs/AlAs SPS's with thin GaAs layers ($m \leq 12$). This indicates that a different scattering mechanism becomes important. Interface scattering due to the interface mixing potential (Γ - X_z mixing) and/or due to potential fluctuations caused by interface roughness (Γ - $X_{x,y}$ mixing) is suggested as a possible mechanism for the Γ - X transfer in the case of the type-II SPS with very thin GaAs layers ($m \leq 12$).

However, it should be pointed out that the present conclusions are based on simple estimates. Nevertheless, the set of data reported here provide a solid and complete base for a much more detailed analysis of this unique scattering process. Such a future analysis possibly has also to include the internal electric field effects neglected completely in our study.

ACKNOWLEDGMENTS

We would like to thank M. Preis and A. Schulz for excellent technical assistance. We gratefully acknowledge the work of A. Fischer and R. Muralidharan with the sample growth. The valuable and helpful discussions with C. Anthony, P. Thomas, and W. W. Rühle are also gratefully acknowledged. The work in Marburg is supported by the Deutsche Forschungsgemeinschaft (Bonn, Germany). Parts of the work in Stuttgart are sponsored by the Bundesministerium für Forschung und Technologie (Bonn, Germany).

- ¹M. Heiblum, M. I. Nathan, D. C. Thomas, and C. M. Knoedler, *Phys. Rev. Lett.* **55**, 2200 (1985).
- ²U. Sivan, M. Heiblum, and C. P. Umbach, *Phys. Rev. Lett.* **63**, 992 (1989).
- ³W. Z. Lin, L. G. Fujimoto, E. P. Ippen, and R. A. Logan, *Appl. Phys. Lett.* **50**, 124 (1987).
- ⁴F. W. Wise, I. A. Walmsley, and C. L. Tang, *Appl. Phys. Lett.* **51**, 605 (1987).
- ⁵R. W. Schoenlein, W. Z. Lin, S. D. Brorson, E. P. Ippen, and J. G. Fujimoto, *Solid State Electron.* **31**, 443 (1988).
- ⁶P. C. Becker, H. L. Fragnito, C. H. Brito-Cruz, R. L. Fork, J. E. Cunningham, J. E. Henry, and C. V. Shank, *Phys. Rev. Lett.* **61**, 1647 (1988).
- ⁷D. N. Mirlin, I. Y. Karlik, and V. F. Sapega, *Solid State Commun.* **65**, 171 (1988).
- ⁸R. G. Ulbrich, J. A. Kash, and J. C. Tsang, *Phys. Rev. Lett.* **62**, 949 (1989).
- ⁹E. Finkman, M. D. Sturge, and M. C. Tamargo, *Appl. Phys. Lett.* **49**, 1299 (1986).
- ¹⁰E. Finkman, M. D. Sturge, M.-H. Meynadier, R. E. Nahory, M. C. Tamargo, D. M. Hwang, and C. C. Chang, *J. Lumin.* **39**, 57 (1987).
- ¹¹G. Danan, B. Etienne, F. Mollot, R. Paniel, A. M. Jean-Louis, F. Alexandre, B. Jusserand, G. LeRoux, J. Y. Marzin, H. Savary, and B. Sermage, *Phys. Rev. B* **35**, 6207 (1987).
- ¹²B. A. Wilson, *IEEE J. Quantum Electron.* **QE-24**, 1763 (1988).
- ¹³K. J. Moore, P. Dawson, and C. T. Foxon, *Phys. Rev. B* **38**, 3368 (1988).
- ¹⁴K. J. Moore, G. Duggan, P. Dawson, and C. T. Foxon, *Phys. Rev. B* **38**, 5535 (1988).
- ¹⁵G. Peter, E. Göbel, W. W. Rühle, J. Nagle, and K. Ploog, *Superlatt. Microstruct.* **5**, 197 (1989).
- ¹⁶B. A. Wilson, C. E. Bonner, R. C. Spitzer, R. Fischer, P. Dawson, K. J. Moore, C. T. Foxon, and G. W. 't Hooft, *Phys. Rev. B* **40**, 1825 (1989).
- ¹⁷P. Dawson, K. J. Moore, C. T. Foxon, G. W. 't Hooft, and R. P. M. van Hal, *J. Appl. Phys.* **65**, 3606 (1989).
- ¹⁸J. Feldmann, R. Sattmann, E. Göbel, J. Kuhl, J. Hebling, K. Ploog, R. Muralidharan, P. Dawson, and C. T. Foxon, *Phys. Rev. Lett.* **62**, 1892 (1989).
- ¹⁹P. Saeta, J. F. Federici, R. J. Fischer, B. I. Greene, L. Pfeiffer, R. C. Spitzer, and B. A. Wilson, *Appl. Phys. Lett.* **54**, 1681 (1989).
- ²⁰J. Feldmann, R. Sattmann, E. Göbel, J. Nunnenkamp, J. Kuhl, J. Hebling, K. Ploog, R. Muralidharan, P. Dawson, and C. T. Foxon, *Solid State Electron.* **32**, 1713 (1989).
- ²¹Y. Masumoto, T. Mishina, F. Sasaki, and M. Adachi, *Phys. Rev. B* **40**, 8581 (1989).
- ²²Hung-Sik Cho and P. R. Prucnal, *Phys. Rev. B* **36**, 3237 (1987).

- ²³F. Minami, K. Hirata, K. Era, T. Yao, and Y. Masumoto, *Phys. Rev. B* **36**, 2875 (1987).
- ²⁴P. Lefebvre, B. Gil, H. Mathieu, and R. Planel, *Phys. Rev. B* **39**, 5550 (1989).
- ²⁵M.-H. Meynadier, R. E. Nahory, J. M. Worlock, M. C. Tamargo, J. L. deMiguel, and M. D. Sturge, *Phys. Rev. Lett.* **60**, 1338 (1988).
- ²⁶N. J. Pulsford, R. J. Nicholas, P. Dawson, K. J. Moore, G. Duggan, and C. T. Foxon, *Phys. Rev. Lett.* **63**, 2284 (1989).
- ²⁷G. Bastard, *Phys. Rev. B* **25**, 7584 (1982).
- ²⁸J. N. Schulman and T. C. McGill, *Phys. Rev. Lett.* **39**, 1681 (1977).
- ²⁹J. Ihm, *Appl. Phys. Lett.* **50**, 1068 (1987).
- ³⁰Yan-Ten Lu and L. J. Sham, *Phys. Rev. B* **40**, 5567 (1989).
- ³¹D. Z. Ting and Y. C. Chang, *Phys. Rev. B* **36**, 4359 (1987).
- ³²M. A. Gell, D. Ninno, M. Jaros, and D. C. Herbert, *Phys. Rev. B* **34**, 2416 (1986).
- ³³L. D. L. Brown, M. Jaros, and D. J. Wolford, *Phys. Rev. B* **40**, 6413 (1989).
- ³⁴D. Scalbert, J. Cernogora, C. B. Guillaume, M. Maaref, F. F. Charfi, and R. Planel, *Solid State Commun.* **70**, 945 (1989).
- ³⁵H. W. van Kesteren, E. C. Cosman, P. Dawson, K. J. Moore, and C. T. Foxon, *Phys. Rev. B* **39**, 13 426 (1989).
- ³⁶P. Dawson, C. T. Foxon, and H. W. van Kesteren, *Semicond. Sci. Technol.* **5**, 54 (1990).
- ³⁷M. S. Skolnick, G. W. Smith, I. L. Spain, C. R. Whitehouse, D. C. Herbert, D. M. Whittaker, and L. J. Reed, *Phys. Rev. B* **39**, 11 191 (1989).
- ³⁸W. H. Knox, C. Hirlimann, D. A. B. Miller, J. Shah, D. S. Chemla, and C. V. Shank, *Phys. Rev. Lett.* **56**, 1191 (1986).
- ³⁹S. Schmitt-Rink, D. S. Chemla, and D. A. B. Miller, *Phys. Rev. B* **32**, 6601 (1985).
- ⁴⁰The split-off band signal is already apparent at negative time delay because of the large chirp of 8 fs/nm in this experiment.
- ⁴¹W. Z. Lin, R. W. Schoenlein, J. G. Fujimoto, and E. P. Ippen, *IEEE J. Quantum Electron.* **QE-24**, 267 (1988).
- ⁴²M. Nakazawa, T. Nakashima, H. Kubota, and S. Seikai, *Opt. Lett.* **12**, 681 (1987).
- ⁴³C. V. Shank and D. H. Auston, *Phys. Rev. Lett.* **34**, 479 (1975).
- ⁴⁴H. J. Eichler, P. Günther, and D. W. Pohl, in *Laser-Induced Dynamic Gratings* (Springer, Berlin, 1985), p. 48.
- ⁴⁵B. R. Nag, in *Electron Transport in Compound Semiconductors*, Vol. 11 of *Springer Series in Solid-State Sciences*, edited by H.-J. Queisser (Springer, Berlin, 1980).
- ⁴⁶J. L. Birman, M. Lax, and R. Loudon, *Phys. Rev.* **145**, 620 (1966).
- ⁴⁷S. Zollner, S. Gopalan, and M. Cardona, *Appl. Phys. Lett.* **54**, 614 (1989).
- ⁴⁸G. R. Olbright, W. S. Fu, J. Klem, A. Owyong, G. R. Hadley, L. Galbraith, R. Binder, and S. W. Koch (unpublished).
- ⁴⁹H. C. Liu, *Appl. Phys. Lett.* **51**, 1019 (1987).
- ⁵⁰W. H. Knox, R. L. Fork, M. C. Downer, D. A. B. Miller, D. S. Chemla, and C. V. Shank, *Phys. Rev. Lett.* **54**, 1306 (1985).
- ⁵¹R. E. Prange and T. W. Nee, *Phys. Rev.* **168**, 779 (1968).
- ⁵²A. Gold, *Phys. Rev. B* **35**, 723 (1987).
- ⁵³J. A. Brum and G. Bastard, *Solid State Commun.* **53**, 727 (1985).
- ⁵⁴F. Stern, in *Physics and Applications of Quantum Wells and Superlattices*, Vol. 170 of *NATO Advanced Study Institute Series*, edited by E. E. Mendez and K. von Klitzing (Plenum, New York, 1987), p. 133.
- ⁵⁵K. Lee, M. S. Shur, T. J. Drummond, and H. Morkoç, *J. Appl. Phys.* **54**, 6432 (1983).
- ⁵⁶P. J. Price, *Ann. Phys. (N.Y.)* **133**, 217 (1981).
- ⁵⁷R. Ferreira and G. Bastard, *Phys. Rev. B* **40**, 1074 (1989).
- ⁵⁸H. Jung, A. Fischer, and K. Ploog, *Appl. Phys. A* **33**, 9 (1984).
- ⁵⁹S. Adachi, *J. Appl. Phys.* **58**, R1 (1985).
- ⁶⁰G. Oelgart, R. Schwabe, M. Heider, and B. Jacobs, *Semicond. Sci. Technol.* **2**, 468 (1987).